Saini et al. present an interesting modeling study in which the authors investigate the response of the global marine ecosystem to an increase in the supply of dust - and by inference Fe – to the ocean surface at the last glacial inception, 70 ka. The scarcity of Fe is indeed considered to limit biological/export production in large swaths of the world ocean, in particular in polar regions today and in the past.

Their sensitivity experiments indicate that increased availability of Fe conduces to a strengthening of the marine biological carbon pump, which contributes to sequester C in the ocean interior, decreasing atmospheric CO2 concentrations (4-16 ppm). What's more, their model outputs suggest that most of the action is centered in the Southern Ocean (SO). Furthermore, the experiments suggest that the strengthening of the biological carbon pump consequent to Fe fertilization rapidly saturates as a result of complex interactions involving downstream effects, to me, the most interesting conclusion of the work.

The study is certainly interesting and worth publishing, yet I feel is it not sufficiently anchored in available palaeoceanographic records. High-resolution EP reconstructions across the MIS4/MIS5 interval are arguably limited, yet available records are often at odds with the model outputs - notably in the subsarctic North Pacific and the SO - which warrants a much more detailed/nuanced discussion. What's more, given the sensitivity of the SO to increased supply of dust/Fe, I would urge the authors to distinguish the SAZ and AZ, as these regions have responded very differently in terms of EP.

We thank the reviewer for their very interesting comments and valuable sources of information for proxy records. We agree that our iron fertilisation discussion should distinguish the responses of the sub-Antarctic zone (SAZ) and Antarctic zone (AZ) in the Southern Ocean. We have now incorporated this suggestion throughout the manuscript and have also provided detailed comparison with the suggested proxy records. As the focus of this paper is on Southern Ocean iron fertilisation and its impact on global CO_2 changes, we do not present a detailed discussion of the changes occurring in the North Pacific. Nevertheless, we have mentioned the differences between our results and the proxy data available in this region.

Please find my comments below, which I hope the authors will find constructive.

l. 39 - Interestingly, d13CO2 data suggest that the drop in atmospheric CO2 centered around 70 kyrs was likely related to a combination of factors including enhanced C storage in the ocean subsurface and decreased air-sea gas exchange in the SO (Eggleston et al., 2016; Menking et al., 2022).

We thank the reviewer for referring these studies. We are now including $\delta^{13}CO_2$ records from Eggleston et al., (2016) and Menking et al. (2022) in Figure 1 (Fig. R2 below) and are discussing their implication in the introduction:

Lines 42-47:

Interestingly, high resolution $\delta^{13}CO_2$ records from Antarctic ice cores (Menking et al., 2022) display a 0.5 permil decrease centred at 70.5 ka, followed by a 0.7 permil increase (Figure R2g), indicating a complex set of processes impacting atmospheric CO_2 at the MIS5-4 transition. While surface ocean cooling could explain the concurrent CO_2 and $\delta^{13}CO_2$ decrease, the $\delta^{13}CO_2$ increase in the second part of the transition would be consistent with a greater efficiency of the biological pump and increased storage of respired carbon in the deep ocean (Menviel et al., 2015, Eggleston et al., 2016, Menking et al., 2022).

l. 49-51 & 227-233 - I find this argument somewhat misleading. I would encourage the authors to discuss the SAZ and AZ separately, as mentioned above. Palaeoceanographic data indeed suggest an increase in EP in the SAZ at the MIS4/5 transition (e.g. Martinez-Garcia et al., 2011/2014; Lamy et al., 2014; Thöle et al., 2019; Amsler et al., 2022). However, palaeoceanographic records from the AZ suggest a simultaneous decrease in EP (e.g. Anderson et al., 2009; Jaccard et al., 2013; Studer et al., 2015; Thöle et al., 2019; Amsler et al., 2022).

We thank the reviewer for this comment. In our model, the 47°S boundary roughly matches with the subantarctic front (SAF) which delineates the subantarctic zone (SAZ) and the Antarctic zone (AZ). Our current description of the results is based on this boundary, north and south of which we see changes of opposite sign. This has been made clearer now using the terms SAF, SAZ and AZ throughout the manuscript.

Lines 55-59:

These peaks in dust flux are concurrent with increased export production (EP) in the subantarctic zone (SAZ) of the Southern Ocean during the LGM (Kohfeld et al., 2005, 2013; Martinez-Garcia et al., 2014), as well as during MIS4 (Lamy et al., 2014; Martinez-Garcia et al., 2014; Thöle et al., 2019; Amsler et al., 2022). On the other hand, palaeoceanographic data from the Antarctic zone (AZ) suggest a decrease in EP at the LGM and MIS4 (Kohfeld et al., 2005,2013; Anderson et al., 2009; Jaccard et al., 2013; Studer et al., 2015; Thöle et al., 2019; Amsler et al., 2022).

Lines 189-196:

Within the AZ (south of the APF), diatoms decrease by 14% in the Pacific, while they increase by 3% in the Atlantic and Indian sectors (Figure A4a). The decrease in diatoms in the Pacific sector of the AZ leads to a competitive growth advantage for coccolithophores, which increase by 6.5% south of the polar front, thus leading to a poleward shift of coccolithophores in the Pacific sector (Figure A4b). On the other hand, coccolithophores decrease in the Atlantic and Indian sectors of the AZ by 15% and 8%, respectively. Diatoms increase by 22% in the SAZ (north of the SAF) while there are no significant changes in coccolithophores abundance. As a result of the changes in these two plankton species, EP increases by 1.3% in the SAZ and decreases by 14% in the AZ (Figure 3b). The total Southern Ocean (south of 30°S) EP and NPP decrease by 2% and 7.5%, respectively at 70 ka.

Lines 225-227:

Our experiments show that the ecosystem response north and south of ~47°S (which is roughly the modern SAF) are of opposite sign (Table 3, Figure 6).

Lines 271-276:

Iron increase in the lambfe3% experiment leads to a 37% increase in diatoms and an 88% increase in coccolithophores in the AZ (Figure A4c, d). The simulated increased EP in the AZ (Figure 5a) leads to greater nutrient utilisation south of the APF (Figure A9c). On the contrary, because of lower nutrient availability, both diatoms and coccolithophores abundances decrease in the SAZ by 46% and 31% respectively (Figure A4c, d). Consequently, in the lambfe3% experiment, the EP increases by 98% in the AZ while it decreases by 17% in the SAZ compared to the 70ka-control simulation (Figure 5a, 6a).

We have also added the following detailed discussion on the model data discrepancy and Fig. R1 as Figure A5b in the appendix:

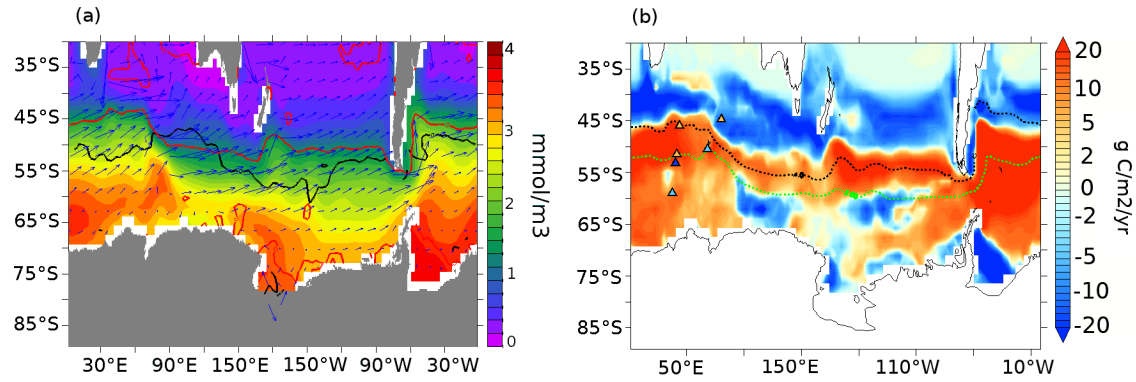

Fig.R1: (a) Surface nitrate concentrations (mmol m^{-3}) for the 70ka-control experiment. The overlaid contours show the zero isoline of annual wind stress curl (black) and the zero contour of EP anomalies (red) between lambfe3% and 70ka-control (pife1%). Blue arrows represent surface currents; (b) Export production anomalies (gC m^{-2} yr^{-1}) at 177.5m depth for lambfe3% compared to PI-control (pife1%) with opal flux (triangles) proxy records from Amsler et al., 2022 (left of 50°E) and from Thöle et al., 2019 (right of 50°E) to show qualitative comparison between model and data. Dark (light) orange represents significantly higher (slightly higher), and dark (light) blue represents significantly lower (slightly lower) values at 70ka compared to PI. Overlaid dashed contours represent modern SAF in black and APF in green based on the definition of Sokolov et al., (2009).

Lines 313-331:

Alkenone flux (Lamy et al., 2014; Martinez et al., 2014), as well as opal and organic carbon fluxes (Thöle et al., 2019) reconstructed from subantarctic sediment cores suggest that EP was higher in the SAZ during MIS4 than present day. In addition, bottom water oxygenation records indicate a deep ocean oxygenation decrease during MIS4, which might suggest increased respired carbon storage in the deep ocean (Amsler et al., 2022) but could also reflect a change in ocean dynamics and water residence time. It has been suggested that the subantarctic EP increase during MIS4 was due to higher iron fluxes into the Southern Ocean. Higher dust deposition in the South Pacific and the South Atlantic at 70 ka is consistent with available paleo-proxy records (Martinez et al., 2011, Lambert et al., 2012, Lamy et al., 2014, Thöle et al., 2019). At the same time, palaeoceanographic records from the AZ suggest a decrease in EP during MIS4 (Anderson et al., 2009; Jaccard et al., 2013; Studer et al., 2015; Thöle et al., 2019; Amsler et al., 2022).

In our 70 ka simulations with enhanced iron input, EP increases in the AZ and polar frontal zone (between SAF and APF) and decreases in the SAZ, in contrast with most paleo-proxy records (Figure A5b). However, there is evidence that greater iron flux within the seasonal sea ice zone has led to higher diatom concentrations (Abelmann et al. [2006, 2015]) and likely also EP in this region during glacial periods. In our study, as the iron input into the ocean increases, the nutrient utilisation increases in the AZ, consistent with the existing $d^{15}N$ records in the AZ at the MIS4/MIS5 transition (Studer et al., 2015; Ai et al., 2020). As a result, the nutrient advection into the SAZ is reduced, thus leading to an EP decrease in the SAZ. In addition, our simulated EP increase in the AZ during MIS4 compared to PI, and thus increase in regenerated carbon storage in the deep ocean, is consistent with some of the proxy records suggesting a decrease in deep ocean oxygenation in the AZ (Jaccard et al., 2016, Amsler et al., 2022). Our EP increase is also consistent with the increase in opal flux north of the APF (Amsler et al., 2022) at the MIS4 onset (Figure A5b).

Fig. 1 – maybe the authors could include ice core d13CO2 data (Eggleston et al., 2016; Menking et al., 2022) in the figure?

We thank the reviewer for this suggestion. Ice core $\delta^{13}CO_2$ data from Eggleston et al., (2016) and Menking et al., (2022) is now added in the Figure 1 in the manuscript as fig. R2. below

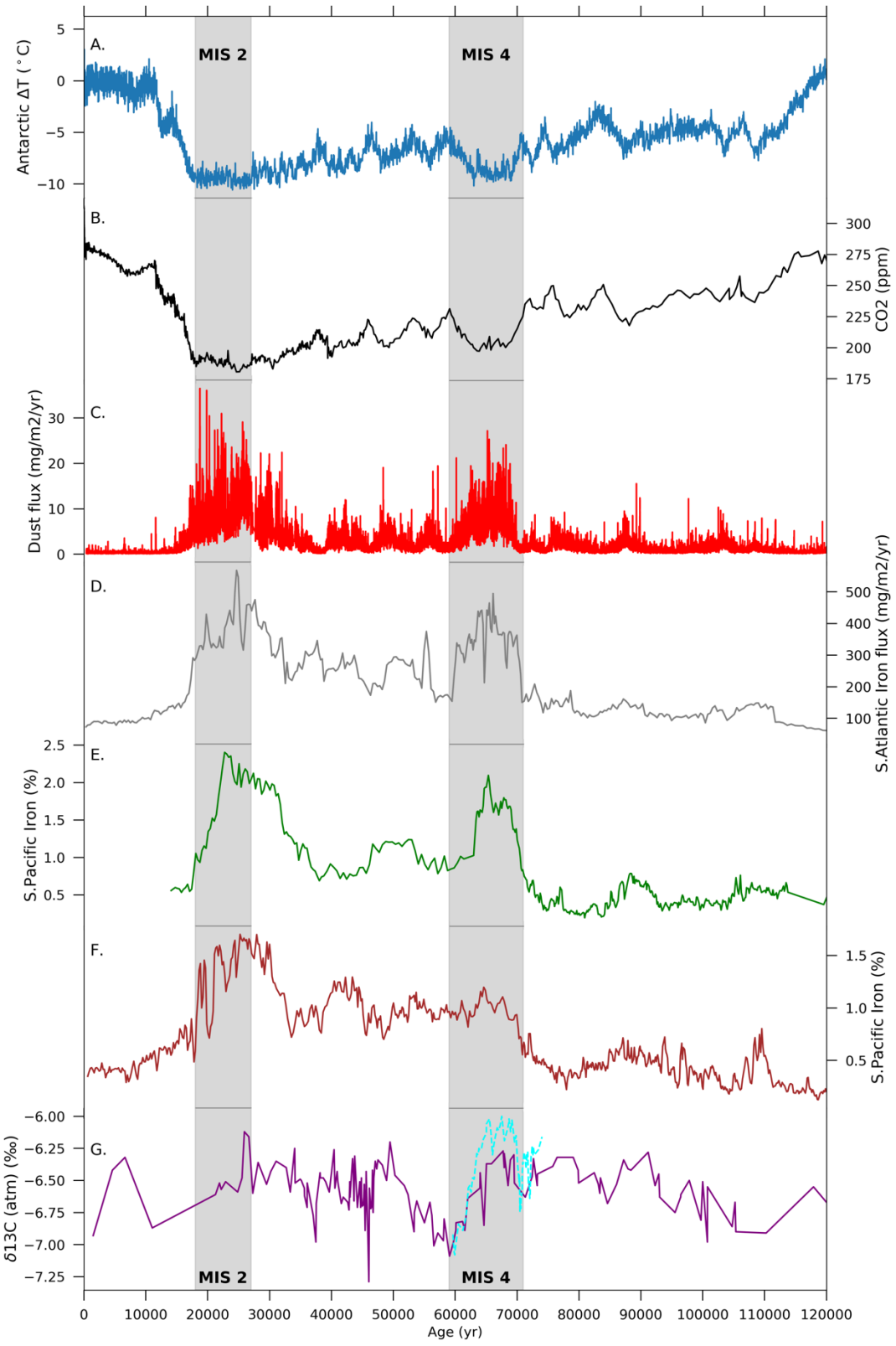

Fig.R2: Time series of (a) Antarctic temperature anomalies from present day (°C) (Jouzel et al., 2007), (b) atmospheric CO_2 concentration (ppm) (Bereiter et al., 2015), and (c) dust flux (mg/m^2/yr) (Lambert et al., 2012) as recorded in EPICA DOME C ice core; (d) iron dust accumulation rates (mg/m^2/yr) from ODP Site 177-1090 (Atlantic) Martinez et al., 2011), iron (%) records in the South Pacific from Lamy et al., (2014) at sites (e) PS75-076 and (f) PS75-059; (g) atmospheric $\delta^{13}CO_2$ (‰) as recorded in a composite of Antarctic ice cores (purple line, Eggleston et al., 2016) and high resolution records from Taylor Glacier ice cores (dashed cyan line, Menking et al., 2022). Shaded areas represent marine isotope stages 2 (MIS2: 27-19 ka BP) and 4 (MIS4: 71-59 ka BP).

l. 92/115 & Table 1 – could the authors provide some more context related to the dust flux estimates used in the simulations? The reason I'm asking is that the reconstructed dust/Fe fluxes to Antarctica based on ice cores measurements are much larger when compared to Fe fluxes quantified based on marine sediments. These differences may relate to different transport pathways and/or atmospheric dynamics over the SO and Antarctica during the last ice age.

The dust flux estimates from Lambert et al. (2015) are globally interpolated 2-d dust flux patterns using the unevenly distributed dust flux data points (including data from both, ice cores and marine sediments), most of them collated in the DIRTMAP (Dust Indicators and Records of Terrestrial and Marine Paleoenvironments) database. Their interpolation method assumes that the aerosol concentration in the air decreases exponentially from the source. On the other hand, dust flux estimates from Ohgaito et al., (2018) were generated by a model, assuming dry and unvegetated regions as dust sources and simulating global dust transport and deposition. Here, both glacfe and lambfe iron fluxes were obtained by mapping the iron content of dust using the estimates of Zhang et al., (2015). We have included this information in the method section.

Lines 103-112:

From this control simulation, we branch off a suite of sensitivity experiments with prognostic atmospheric CO_2, using two different glacial iron dust flux estimates. The first iron flux, lambfe, is obtained from the LGM dust estimates of Lambert et al., (2015). This dust flux estimate is calculated by performing a global 2-d interpolation on unevenly distributed LGM dust flux records, most of which are collated in the DIRTMAP (Dust Indicators and Records of Terrestrial and Marine Paleoenvironments) database (Kohfeld and Harrison, 2001; Maher et al., 2010). Their interpolation method assumes that the aerosol concentration in the air decreases exponentially from the source distance. The second iron flux, glacfe, is derived from a dust flux obtained with a model (LGMglac.a, Ohgaito et al., (2018)). This model includes glaciogenic dust sources in addition to the usual desert dust sources and assumes dry and unvegetated regions as dust sources. It then calculates global dust transport and deposition. Both glacfe and lambfe are then obtained in this study by mapping the iron percentage on dust (Zhang et al., 2015) as mentioned above.

l. 150 – is the AMOC both weaker and significantly shallower in the 70 kyr simulation?

As seen in Fig. R3 (now added as Fig. A3 in the appendix), the AMOC is not significantly shallower in the 70ka simulation compared to PI.

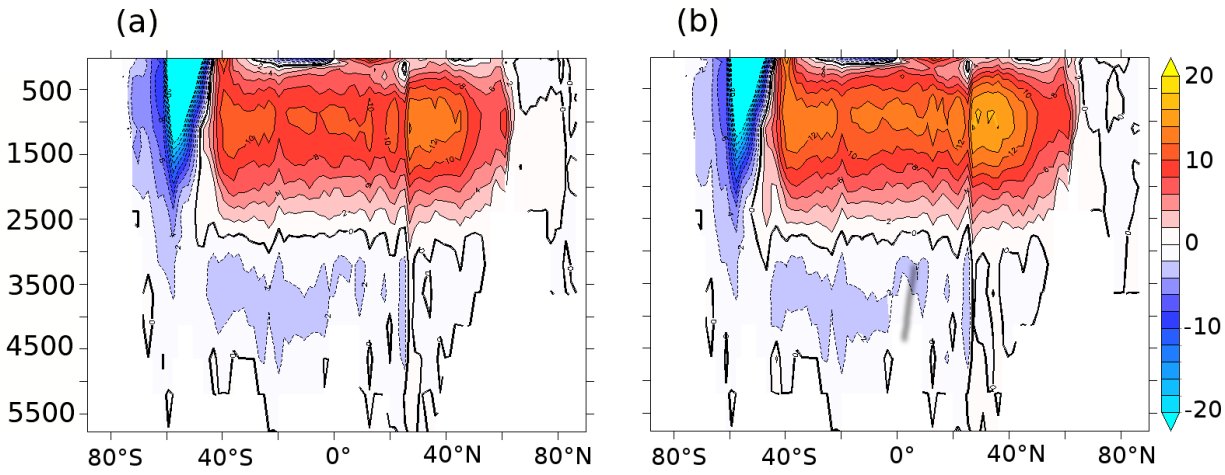

Fig. R2: Atlantic meridional overturning streamfunction (Sv) at (a) 70 ka BP and (b) PI.

We also add this information as below:

Line 178:

The simulated AMOC strength in the 70ka-control experiment is ~14Sv, compared to ~17Sv in the PI-control, without significant changes in its depth.

l. 154-156 & 234-236 - Interesting… but these observations seem at odds with paleoceanographic reconstructions, which generally show a decrease in EP at the MIS4/MIS5 transition (e.g. Jaccard et al., 2005; Gebhardt, et al., 2008). These observations are consistent with paleoceanographic reconstructions spanning the last deglaciation, which consistently indicate lower EP during the LGM, even though Fe supply might have been higher then (e.g. Kohfeld & Chase, 2011 for a review)

We thank the reviewer for this comment and providing us with these references. The simulated increase in EP in the North Pacific is due to greater NO_3 availability in our 70ka-control simulation; caused by higher denitrification in the North Pacific in our PI-control simulation. This leads to an increase in diatoms and coccolithophores in this region and thus EP.

However, as this study focuses on iron fertilisation in the Southern Ocean, we did not discuss results from the North Pacific in detail especially for differences between 70ka and PI climate which use the same iron masks and iron solubility factor. We now mention this model data discrepancy in the paragraph as below:

Lines 183-187:

The simulated 18% EP increase at 70 ka in the North Pacific (Figure 3b) can be attributed to greater diatom and coccolithophore abundance in that region (Figure A4a, b), resulting from higher nutrient availability. This EP increase in the North Pacific is however inconsistent with the biogenic Ba (Jaccard et al., 2005) and $d^{15}N$ (Gebhardt et al., 2008) records from the sub-arctic North Pacific which suggest a decrease in EP at MIS4 onset.

l. 153 – I'm not sure to understand what is meant by "strength of the deep water masses"?

We have modified this sentence as below:

Line 181:

The colder conditions, more extensive sea-ice cover, and changes in the deep ocean convection impact marine productivity (Saini et al., 2021).

l. 156 – what do you mean by "general phytoplankton"?

There are four different classes for phytoplankton in the ecosystem model used in this study. Three of which include specifically characterized plankton such as diazotrophs, that can fix nitrogen, coccolithophores, that produce $CaCO_3$ shells, and diatoms that produce opal. The fourth class is for the rest of the types of plankton, that are mostly located in the low latitude regions. This is now explicitly described in the manuscript:

Lines 84-87:

There are four different classes for phytoplankton in this ecosystem model. Three of which include specifically characterized plankton such as diazotrophs that can fix nitrogen, coccolithophores that produce $CaCO_3$ shells, and diatoms that produce opal. The fourth class is for the rest of the types of plankton, that are mostly located in the low latitude regions.

l. 157-163 – again, I would recommend discussing the SAZ and AZ separately.

We have now included this information as below:

Lines 173-176:

The strongest ocean surface cooling (-1.45°C) at 70 ka BP with respect to our PI-control is simulated north of 40°N in the Atlantic and Pacific oceans, while the annual mean SSTs in the SAZ and AZ are ~0.8°C and 0.4°C lower than in the PI-control, respectively (Figure 3a).

l. 168-169 – why is that? Are ecosystems rapidly becoming N-limited as Fe availability increases?

Yes, the ecosystem becomes nitrate limited in the northern band of the Southern Ocean as iron flux increases in our simulations.

We are now including an analysis of the factors limiting the growth rate of diatoms and coccolithophores in the Southern Ocean.

Photosynthesis in this model is calculated by multiplying the concentration of the phytoplankton functional type in question with the minimum of three/four terms which are light, nitrate and phosphate for coccolithophores, and additionally silicate for diatoms (Equations 13-16 in Kvale et al., 2021). Please note that nitrate limitation depends on nitrate concentration scaled by iron availability and ocean temperature (Equations 3 and 5 in Kvale et al., 2021). The same is true for phosphate and silicate limitation. The light limitation includes light attenuation by plankton biomass and sea ice cover (Equation 12 in Kvale et al., 2021) and is also scaled by temperature and iron availability (Equation 9 in Kvale et al., 2021). In Fig. R2 and R3 we show Hovmöller diagrams showing the seasonal evolution of the proportion of ocean grid cells at each latitude band that are limited by each of these factors for diatoms and coccolithophores in our simulations.

At low iron levels (our 70ka-control run, Fig. R2, added as Figure A9 in the manuscript), light limits the growth of coccolithophores and diatoms south of ~75°S throughout the year (Fig. R2a, c), while nitrate

limits the growth of these plankton functional types in more than 80% of the cells north of ~40°S (Fig. R2b, d). In the band between ~40°S and ~75°S, the limitation moves back and forth between light and nitrate for coccolithophore growth (Fig. R2a, b) and between light, nitrate, and silicate for diatom growth (Fig. R2c-e). Phosphate only limits the plankton growth in the 70ka-control run for a very short time at the northern boundary of our region of interest (~20°S). We therefore concentrate on nitrate and silicate in our analysis.

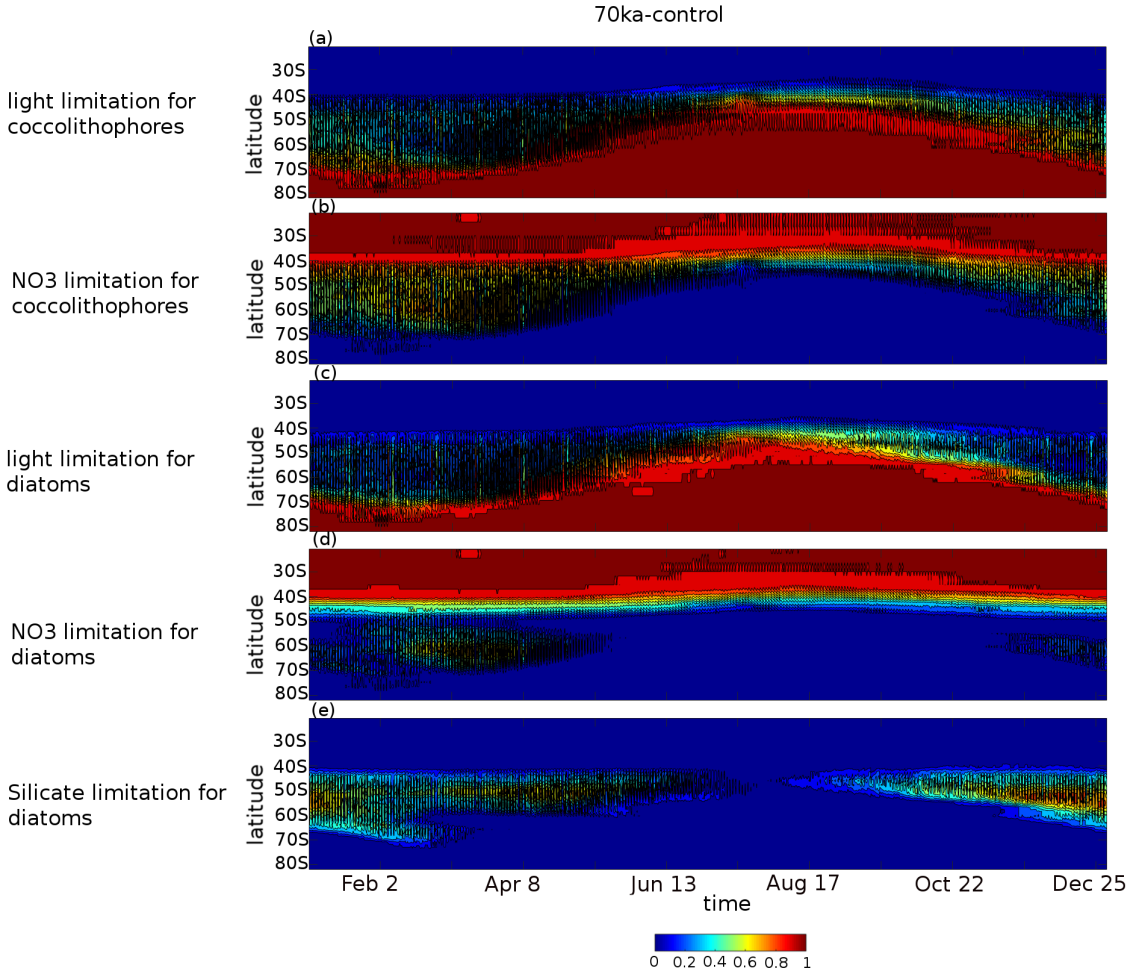

Fig.R2: Hovmöller diagrams of the proportion of ocean grid cells per latitude band for the 70ka-control experiment for which (a) light is limiting coccolithophore growth (b) nitrate is limiting coccolithophore growth, (c) light is limiting diatom growth (d) nitrate is limiting diatom growth, (e) silicate is limiting diatom growth. In all the subpanels, if shade=1, then all ocean grid cells at that latitude band are limited by the respective limiting factor, if shade=0.5, then half of them are.

To illustrate the changes occurring as more iron is added into the Southern Ocean, we show the changes in the proportion of ocean cells limited by each factor in experiment lambfe20% compared to the 70ka-control (Fig. R3, added as Figure A10 in the manuscript). The region between 40°S and 50°S becomes significantly more nitrate limited for both coccolithophores and diatoms in the lambfe20% experiment (Fig. R3a, b). With higher iron availability, NPP and export production south of 47°S increases, using nutrients more efficiently (Fig. R1c, now added as Figure A9c in the appendix) and reducing the northward nutrient advection (Fig. R1b, now added as Figure A9b in the appendix). At the same time silicate limitation for diatoms decreases in this region (Fig. R3c). This is because, as

the iron flux increases, both coccolithophores and diatoms shift southward leading to a decrease in diatoms between 40°S and 55°S. This further enhances silica availability in this region, consequently leading to a decrease in silicate limitation.

We also show the proportion of ocean cells that are limited by either of the macronutrients (nitrate or phosphate for coccolithophores; and nitrate, phosphate, or silicate for diatoms) in Fig. R3d and e. In this figure we see that the overall nutrient limitation between ~40°S and 50°S increases in the high iron flux experiment compared to 70ka-control.

Therefore, in agreement with the reviewer's comment, we now state that the saturation in the biological pump is indeed due to nitrate limitation in the northern band of the Southern Ocean as the iron fluxes increase.

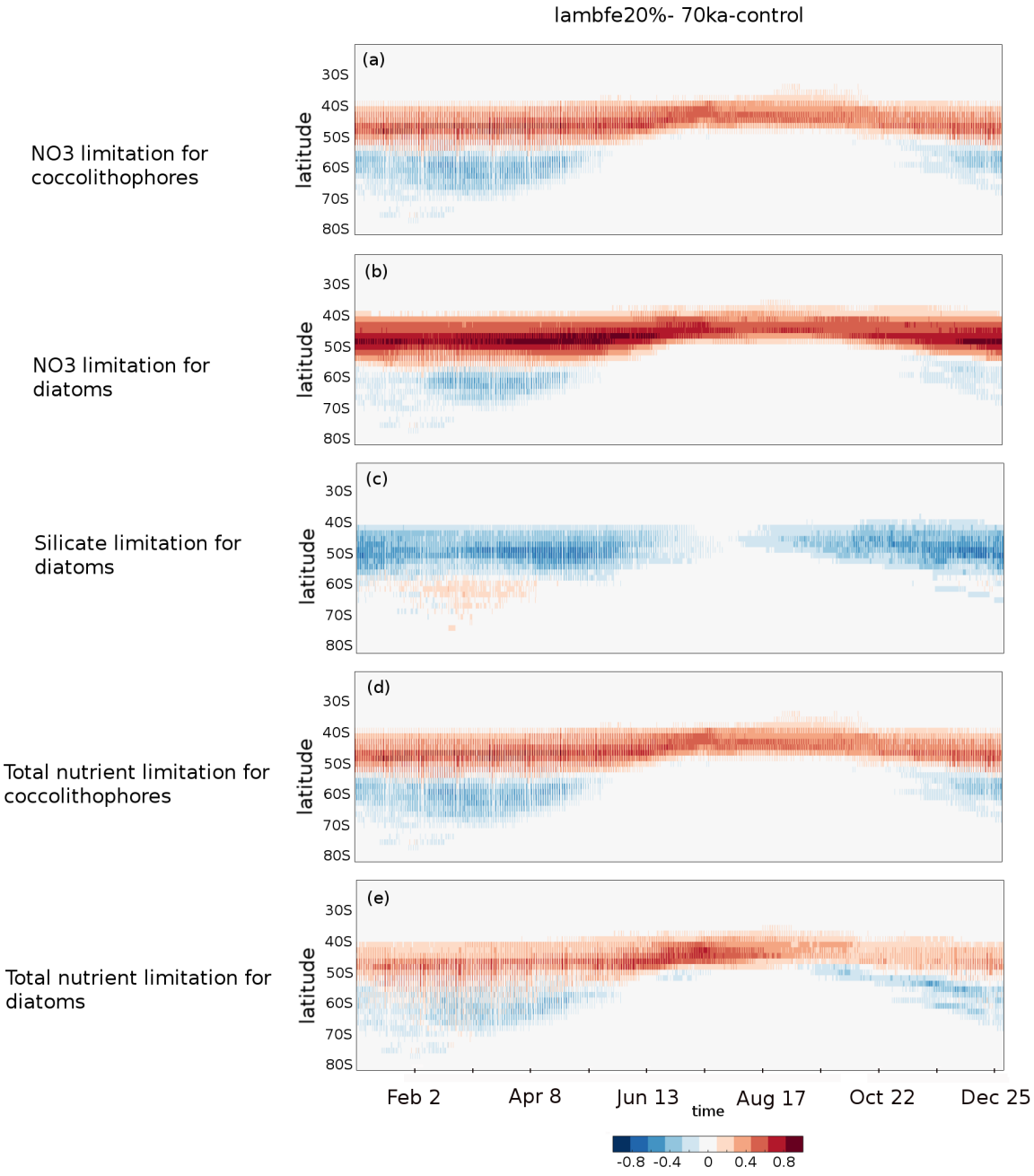

Fig.R3: Hovmöller diagrams of the lambfe20% minus 70ka-control anomaly in the proportion of ocean grid cells per latitude band for which (a) nitrate is limiting coccolithophore growth, (b) nitrate is limiting diatom growth, (c) silicate is limiting diatom growth, (d) either of the macronutrients is limiting coccolithophore growth and (e) either of the macronutrients is limiting diatom growth.

We now include this information as the following text and as Figures A9 and A10 respectively.

Lines 244-253

However, as the Southern Ocean iron flux increases, the overall iron fertilisation efficiency reduces. While export production increases south of 47°S, thus using nutrients more efficiently (Figure A8c) and reducing the nutrient advection north of the SAF (Figure A8b), nitrate limitation increases in the sub-Antarctic zone (Figure A9b, d and Figure A10a, b), leading to a decrease in export production. For example, in experiment lambfe20%, a 67% decrease in nitrate concentration is simulated between 40°S and 47°S (Figure A8b). At the same time, silicate limitation decreases in the sub-Antarctic zone (Figure 9e and Figure A10c) due to a southward shift of both coccolithophores and diatoms and a decrease in diatoms between 40°S and 55°S (Figure A11). This further enhances silica availability in this region, consequently leading to a decrease in silicate limitation. Therefore, the total biological pump efficiency, represented here by changes in P* (Figure 4c) and Southern Ocean EP to NPP ratio (Figure A8a), saturate at high iron values due to nitrate limitation north of 50°S in the Southern Ocean. The global P* in lambfe20% and in lambfe50%-47S (Figure 4c) equal 0.63 and 0.65 respectively, suggesting a maximum efficiency of 65% in our experimental set-up.

l. 178-182 & 283 – This is not really surprising as EP was likely limited by the scarcity of N (or P) outside of the SO during the last ice age.

We agree with this comment. Here, we are only emphasizing the latitudinal region within the Southern Ocean which is most sensitive to iron fertilisation.

l. 179-188 – this conclusion is at odds with existing paleoceanographic reconstructions. Data suggest that the SAZ was particularly responsive to aeolian Fe supply, while ecosystems in the AZ mainly responded to (micro)nutrient supply from below via upwelling and vertical mixing (e.g. Jaccard et al., 2013). Moreover, N-isotope data suggest that the relative uptake of nitrate increased both in the SAZ (Martinez-Garcia et al., 2014) and the AZ (Studer et al., 2015; Ai et al., 2020) at the MIS4/MIS5 transition.

We thank the reviewer for this comment. Please note that in this section we are discussing differences between two 70 ka BP simulations and not the differences between 70 ka BP and PI. However, we agree with the reviewer's comment that our results are inconsistent with some of the available paleo records. The explanation behind this is now added in the discussion:

Lines 317-339:

Alkenone flux (Lamy et al., 2014; Martinez et al., 2014), as well as opal and organic carbon fluxes (Thöle et al., 2019) reconstructed from subantarctic sediment cores suggest that EP was higher in the SAZ during MIS4 than present day. In addition, bottom water oxygenation records indicate a deep ocean oxygenation decrease during MIS4, which might suggest increased respired carbon storage in the deep ocean (Amsler et al., 2022) but could also reflect a change in ocean dynamics and water residence time. It has been suggested that the subantarctic EP increase during MIS4 was due to higher iron fluxes into the Southern Ocean. Higher dust deposition in the South Pacific and the South Atlantic at 70 ka is consistent with available paleo-proxy records (Martinez et al., 2011, Lambert et al., 2012, Lamy et al.,

2014, Thöle et al., 2019). At the same time, palaeoceanographic records from the AZ suggest a decrease in EP during MIS4 (Anderson et al., 2009; Jaccard et al., 2013; Studer et al., 2015; Thöle et al., 2019; Amsler et al., 2022).

In our 70 ka simulations with enhanced iron input, EP increases in the AZ and polar frontal zone (between SAF and APF) and decreases in the SAZ, in contrast with most paleo-proxy records (Figure A5b). However, there is evidence that greater iron flux within the seasonal sea ice zone has led to higher diatom concentrations (Abelmann et al. [2006, 2015]) and likely also EP in this region during glacial periods. In our study, as the iron input into the ocean increases, the nutrient utilisation increases in the AZ, consistent with the existing $d^{15}N$ records in the AZ at the MIS4/MIS5 transition (Studer et al., 2015; Ai et al., 2020). As a result, the nutrient advection into the SAZ is reduced, thus leading to an EP decrease in the SAZ. In addition, our simulated EP increase in the AZ during MIS4 compared to PI, and thus increase in regenerated carbon storage in the deep ocean, is consistent with some of the proxy records suggesting a decrease in deep ocean oxygenation in the AZ (Jaccard et al., 2016, Amsler et al., 2022). Our EP increase is also consistent with the increase in opal flux north of the APF (Amsler et al., 2022) at the MIS4 onset (Figure A5b).

l. 211 - does the reduction in terrestrial vegetation and soil moisture imply more dust production (positive feedback)?

We thank the reviewer for this interesting comment. This could indeed be positive feedback. However, this feedback is not included in our simulation as the dust flux is a forcing. This would be an interesting topic for future studies.

l. 247 – these observations would be consistent with a general decrease in deep ocean oxygenation at the onset of MIS4 (e.g. Jaccard et al., 2016; Amsler et al., 2022).

We thank the reviewer for pointing this information. It is now included in the discussion as below:

Lines 336-339:

In addition, our simulated EP increase in the AZ during MIS4 compared to PI, and thus increase in regenerated carbon storage in the deep ocean, is consistent with some of the proxy records suggesting a decrease in deep ocean oxygenation in the AZ (Jaccard et al., 2016, Amsler et al., 2022). Our EP increase is also consistent with the increase in opal flux north of the APF (Amsler et al., 2022) at the MIS4 onset (Figure A5b).